Modeling of inhaled corticosteroids delivery for topical croup treatment in pediatric upper airways

Wang, Yusheng, Ma, Ruiping, Sun, Siping, Hu, Zhenzhen, Li, Chaofan, Lou, Miao, Gong, Minjie, Tong, Zhenbo, Yang, Feilun, Chen, Jingguo, Zheng, Guoxi, Dong, Jingliang and Zhang, Ya (2023) Modeling of inhaled corticosteroids delivery for topical croup treatment in pediatric upper airways. Journal of Drug Delivery Science and Technology, 85. ISSN 1773-2247 (In Press)

Modeling of inhaled corticosteroids delivery for topical croup treatment in pediatric upper airways

Yusheng Wang [a,#], Ruiping Ma [a,#], Siping Sun[b], Zhenzhen Hu [a], Chaofan Li [c], Miao Lou [a], Minjie Gong [a], Zhenbo Tong [e], Feilun Yang [a], Jingguo Chen[a], Guoxi Zheng [a,*], Jingliang Dong [d,*], and Ya Zhang [a,*]

[a] Department of Otolaryngology Head and Neck Surgery, The Second Affiliated Hospital of Xi'an Jiaotong University, Xi'an 710000, China; katherina6870@stu.xjtu.edu.cn (Y.W.); ma315182949@stu.xjtu.edu.cn (R.M.); huzhenzhen@stu.xjtu.edu.cn(Z.H.); loumiao.123_2006@stu.xjtu.edu.cn (M.L.); gmj0517@stu.xjtu.edu.cn (M.G.); yangfeilun@xjtu.edu.cn (F.Y.); jing-guo.chen@xjtu.edu.cn (J.C.)

[b] ZHEJIANG CUIZE PHARMATECH CO., LTD, ssp@cuizepharma.com

[c] Department of Oncology, The Second Affiliated Hospital of Xi'an Jiaotong University, Xi'an 710000, China; (C.L.); 2287151854@qq.com

[d] Institute for Sustainable Industries & Liveable Cities, Victoria University, PO Box 14428, Melbourne, VIC, 8001, Australia; jingliang.dong@vu.edu.au (J.D.)

[e] School of Energy and Environment, Southeast University, Nanjing 210096, China; z.tong@seu.edu.cn (Z.T.);

* Correspondence: zhengguoxi888@sina.com (G.Z.); jingliang.dong@vu.edu.au (J.D.); zhangya@xjtu.edu.cn (Y.Z.); Tel.: +86-135-0918-6588 (G.Z.); +61-3-99195622(J.D.); +86-151-0296-6990 (Y.Z.)

Abstract

Croup is the most frequent cause of pediatric upper airway obstruction characterized by spindle-shaped stenosis in the subglottis mucosa. Inhaled corticosteroids (ICSs) serve as the first-line therapy for croup. Traditional ICS particles (1-4 μm in diameter) are primarily designed for trachea and lung diseases and show extremely low larynx deposition. Moreover, the specific correlation between airway minimal cross-sectional area (CSA) and airway resistance has not been fully understood. In this study, three healthy pediatric upper airway models with commercial nebulizer masks attached to their faces were reconstructed from computed tomography (CT) scans. Virtual mild, moderate, and severe croup were incorporated into these healthy models. To enhance the performance of conventional nebulizing drug delivery, the aerodynamic properties of croup with different degrees of stenosis were quantitatively analyzed, and the respiratory transit and deposition of ICS particles sized between 1 to 20 μm in our target area (glottis+subglottis) were modeled utilizing the Computational Fluid Particle Dynamics (CFPD) method. Results showed that in all models, maximum deposition fractions (DF) can be reached when the ICS particle sizes are 7-8 μm, and for particles sized at 8 and 9 μm, all models can achieve effective target area delivery (≥75% of the maximum DF), whereas the majority of traditional nebulizers produce smaller particles than what we recommended. Pediatric upper airway resistance is negatively correlated with the minimum airspace CSA (R ∝ CSA^{-1}), which is in good agreement with the Bernoulli Obstruction Theory. Furthermore, when the constriction of the subglottis reaches a specific level (≥70% obstruction), the upper airway pressure drop abruptly surged and the dyspneic respiration symptoms of patients develop instantly.

Keywords: Computational fluid particle dynamics (CFPD), croup, inhaled corticosteroids (ICS), particle deposition, pediatric upper airway

1. Introduction

Croup, also known as acute laryngotracheitis, or subglottic laryngitis, is one of the most

1

prominent causes of acute respiratory distress in young children[1], affecting about 15% of children at some point [2]. It most commonly occurs in pediatric between 6 months and 5 years of age[3]. As a result of the upper airway constriction, croup is distinguished by its transient onset of a characteristic barky cough that is typically coupled with stridor, hoarse voice, and even respiratory distress, with endoscopic examination showing subglottic stenosis (SGS)[4,5]. Many treatments are available, including nebulized epinephrine, corticosteroid therapy, oxygen administration, analgesics, decongestants, antibiotics, antipyretics, short-acting β2 agonists, antitussives, and even tracheotomy[1,6]. Regardless of the clinical severity, corticosteroids are the cornerstone of croup therapy[7] as an effective method and are advised by all specialists[8-10]. Treatment with corticosteroids reduces the need for intubation in children with severe croup and impending respiratory failure by about five times, and if they are intubated, they stay intubated for about a third less time and are seven times less likely to necessitate reintubation than kids who are not given this medications[11].

The effectiveness of corticosteroid therapies, including intramuscular dexamethasone[12], oral prednisolone[11], and nebulized budesonide[13], in patients hospitalized for croup, has been firmly established and verified. Inhaled corticosteroids (ICS), especially budesonide, performed remarkably in lowering inflammatory cytokines in the blood and enhancing life quality while maintaining a favorable safety profile in children with croup[14]. It begins to act as early as one hour after administration[15] and is broadly accepted and frequently used as a topical non-invasive approach. Aerosol treatment shows the fundamental privilege of delivering highly concentrated localized medication right to the site of action[16]. The aerosolized medications can be delivered to the human airway through several methods: face mask, mouthpiece, nasal mask, and high-flow nasal cannula. However, the mouthpiece achieves low efficiency for young children due to their poor compliance, and aerosol delivery using the nasal mask was tested to be less effective than using the facemask in an in vitro study among simulated young children who breathed spontaneously[17], therefore the face mask is the most widely used device during pediatric aerosol therapy. It is believed that the inlet cross-section of a nebulizer, the inhaled particle sizes, the airway diameter, and inhalation rates all have impacts on where the deposited inhaled particle located along the airway. [18-21]. Surprisingly, there have no numerical simulation ever explored the application of face masks in the human airway. In consequence, this study looked especially into the delivery of aerosolized using the face mask, and investigated the effect of inhaled particle sizes and the airway diameters on drug delivery efficiency.

Tracking particle deposition and their trajectories along the respiratory tract was made possible by numerical simulations that employ the Computational Fluid Particle Dynamics (CFPD) approach. The effectiveness of medication delivery and the spatial distribution of particle deposition is significantly influenced by their aerodynamic diameter. Small particles (<2 μm) tend to deposit mostly in the pulmonary alveoli district, large particles (>6 μm) deposit primarily in the upper airway, while medium particles (2-6 μm) deposit most in small and central airways[22,23]. Superior olfactory deposition[24] was studied utilizing the breath-powered drug delivery approach and peaking deposition fraction (DF) could be reached with 1 nm diffusive particles and 10μm inertial particles. Sun, QY et al.[25] focused on nanoparticle aerosol delivery in pre-and post-operative nasal airway models of a child with adenoid hypertrophy. Perkins EL et al.[26] utilized the CFPD approach to simulate the inhaled drug particles treating, especially vocal fold granulomas and identified the effective particle sizes for large, medium, and small granulomas are 7-14, 7-13, and

95 6-10 μm, respectively, implying that inhalers generating larger sizes of particles may result in more effective laryngeal drug deposition. When it comes to laryngotracheal stenosis, it was discovered that for all kinds of stenosis, the maximal deposition could be obtained when particle sizes were 6-10 μm, except for one-level tracheal stenosis[27]. By proposing the point-source aerosol release (PSAR) method, Wang et al.[28] managed to target drug delivery to deeper small airways in different lung

100 lobes in pediatric patients with bronchopneumonia. Nevertheless, topical ICS particle delivery aimed at the subglottis region for the treatment of croup has not yet been documented. The aerodynamic diameters of the particles in commercially prescribed nebulizers range between 1 to 4 μm. To date, the ideal qualitative and quantitative features of nebulizers targeting the croup treatment have not reached any consensus. Data evaluating the laryngeal deposition as well as the most effective inhaled

105 particle sizes are necessitated due to the growing clinical usage of ICS drugs. Therefore, a thorough understanding of the respiratory flow pattern and how inhaled particles move through the respiratory tract plays a fundamental role in illness management and associated inhalation therapy. Additionally, most pediatric medications in use today were not created or developed specifically for children, and little was known about pediatric targeted drug delivery. Children are not adults in miniature, they

110 differ tremendously from adults in terms of physiological characteristics, airway anatomy, and breathing patterns[29]. Children also have unique needs for dosage forms and medical delivery systems. To obtain the optimum efficacy drug delivery targeting the croup, we must design the nebulized device specifically for pediatrics with the ideal size of the ICS particles.

Within the larynx, the glottis constricts the upper airways to a minimum transitional

115 cross-section, and mucosal oedema in this site will result in a considerable reduction in cross-sectional area (CSA), manifesting with higher airway resistance (R) and the resulting increased breathing efforts in moderate to severe croup[10,30]. Croup is characterized by spindle-shaped SGS. Clinical assessment is necessary to evaluate the severity of the disease, the existing grading criteria rely solely on the subjective clinical symptoms[1], and there is no quantitative evaluation of croup.

120 The Cotton-Myer classification system[31], which uses laryngoscopy to quantify the percent area of obstruction (% AO) of the lumen at the subglottis and categorizes obstruction severity as: Grade 1, <50% AO; Grade 2, 51–70% AO; Grade 3, 71–99% AO; and Grade 4, total obstruction, is the prevalent criterion assisting the grading and therapy of SGS. However, airway resistance and airspace CSA has a complex interaction that is yet not fully understood. In the context of croup, we

125 attempt to examine the association between disease severity (various degrees of SGS) and pediatric upper airway resistance. Several earlier studies employed the assumption that the Hagen-Poiseuille equation[32] can best explain the human upper airway pressure-flow relationship in the presence of SGS, which states that airflow resistance is negatively correlated with the quartic of the airway lumen diameter, suggesting the resistance was negatively correlated with the quadratic of the airway

130 minimum CSA ($R \propto CSA^{-2}$). On the contrary, other studies demonstrate that the Bernoulli Obstruction Theory[33,34] can explain the upper airway resistance in a more accurate manner, which states that airflow resistance is negatively correlated with the minimum airway CSA ($R \propto CSA^{-1}$).

On top of the existing Cotton-Myer classification system, this study stepped further and virtually simulated three degrees of spindle-shaped SGS: mild croup (30% AO); moderate croup (50%

135 AO); and severe croup (70% AO). Based on the subjects with three levels of stenosis (three severities of croup), the correlation between the resistance of pediatric upper airway and airway minimum CSA was systematically investigated. Further, the CFPD approach was employed to model and assess ICS deposition in the targeted glottis and subglottis regions over a broad scope of particle

3

sizes (1-20μm) so as to explore particle size ranges that may lead to effective deposition in the target area (glottis+subglottis). In most former studies, the cylindrical segments with varying diameters were constructed to simulate various degrees of airway obstruction, the other studies directly inserted a plane to block the airway, and most of them studied a single case. It is worth noting that our study established spindle-shaped stenosis in three healthy children which is more consistent with clinical conditions and more statistically significant.

2. Materials and Methods

2.1. Construction of Base Models

This study was authorized by the medical ethics council and institutional review board of the Second Affiliated Hospital of Xi'an Jiaotong University (batch number: 2022186). We recruited children volunteers aged 4-5 years who were physically fit and had not experienced any respiratory illnesses recently (six months prior to this research), such as pneumonia, rhinitis, tracheobronchitis, tonsillitis, or any other upper airway diseases. Finally, three healthy children were eligible for inclusion in the study. Siemens Dual Source photon computed tomography (CT) scanning was performed on them for an airway scope extending from the mouth to the trachea. During the scanning procedure, the participants had to keep their mouths open and retain their end-inspiratory position with nebulizer face masks attached to their faces. The CT images were then transported, edited, and de-identified in Mimics 19.0 software to reconstruct three-dimensional (3D) models of healthy pediatric upper airways (base models), and then exported in stereolithography (STL) format. Smoothing and regional division were achieved using Geomagic Wrap 2015 software, then each model was divided into 14 parts according to the anatomical structures (Fig. 1A), including face, oral cavity, teeth+cheek, tongue, soft palate, tonsil, nasopharynx, oropharynx, hypopharynx, epiglottis, supraglottis, glottis, subglottis (the area where stenosis occurred), trachea. The airway geometries were imported into ANSYS ICEM-CFD 2021 R1 and Fluent-Meshing 2021 R1 software to produce hexahedral cells with five prism layers (Fig. 1B). Glottis and subglottis regions were combined to be regarded as the "targeted area" to determine the optimal ICS particle sizes. To better describe the procedure for base model construction and data collection, a flow chart was plotted (Fig.2).

2.2. Construction of the stenosis models with various severities of croup

The subglottis from the base models were rescaled to form spindle-shaped stenosis as a way to simulate airway obstruction. Three different croup severities were modeled: mild, moderate, and severe, with 30%, 50%, and 70% AO, respectively, for 30%-70% AO encompassing the Grade 1 to Grade 3 stenosis defined by the Myer-Cotton system. Patients with Myer-Cotto's Grade 4 SGS (total obstruction) generally necessitate tracheotomy or open airway reconstruction, therefore the OA over 70% was not studied in the present study for lack of clinical application value. The length of the obstructed subglottis was unified to be 5mm in each model as it represents the most common situation clinically. Other lengths of stenosis were not further investigated because previous study have proved that the obstruction length showed no significant influence on tracheal resistance with various obstruction diameters at the % AO values analyzed in this study[34]. Detailed processes and methods to construct virtual stenosis are illustrated in Fig. 3.

2.3 CFPD Simulations

Fluent 2021 R1 software (ANSYS, Inc.) was employed to implement steady-state airflow that

was comparable to resting respiratory conditions. The tidal volume and respiratory rate of children were obtained based on published respiratory parameters [35]. 2.7s was set as one breathing cycle in this study[36], and the inspiratory breathing rates of children aged 4-5 years at steady-state breathing were calculated to be 9.03, and 9.77L/min, respectively. To precisely represent the transitional airflow in the pediatric upper airways, a robust turbulent model is absolutely vital. In this community, the Reynolds-Average Navier-Stokes (RANS) approach is generally employed [37]. When it comes to simulating the laminar-transitional-turbulent airflow, the low-Reynolds number k-omega model was proven to be outstanding based on the research of Zhang and Kleinstreuer et al.[38], which evaluated the transitional flow in a restricted tube using four distinct RANS turbulence models, and it was verified to be able to assess the velocity profiles, pressure drop, and shear stress from transition to turbulent flows in a precise manner [36,39]. Therefore, the transition shear stress transport (SST) k-omega model with low Reynolds number correction was used in this study to simulate the aerodynamic characteristics of the pediatric upper airways. The boundary conditions in this article were as follows: 1) Outlet velocities were computed using the flow rate and the trachea CSA of each model. 2) The inlet pressure at the inhalation face mask's entry was set to 0 Pa with the assumption that it was exposed to the atmosphere. 3) The "trapped wall" was determined to be the boundary condition for the particle-wall interaction, suggesting the airway surface would catch particles at initial contact. 4) The models' boundaries were set as no-slip conditions, which meant that the wall's velocity was zero. The airflow during steady-state inhalation was calculated with a second-order upwind algorithm, and the governing equations were incompressible viscous fluid Navier-Stokes equations.

Three degrees of % AO were constructed based on three base models to generate nine unique airway models with virtual stenosis, plus three base models representing non-pathologic airways (12 airway models in total). The detailed demographics, inhalation rate, airway minimal CSA, and pressure drop information of the 12 models were illustrated in Table 1.

2.4. Airway resistance

The definition of airway resistance was $R = \Delta P/Q$, where Q is the inhalation rate and ΔP is the pressure drop from the inlet of the face mask to the outlet in our study.

The pressure-flow connection of the upper airway was explained by two opposing hypotheses in humans with SGS: the Hagen-Poiseuille equation and the Bernoulli Obstruction Theory.

Hagen-Poiseuille equation[32,40] predicts that when fluid in the horizontal circular tube to do the laminar flow movement, its volume flow rate Q follows the equation:
$$Q=\pi \times r^4 \times \Delta p/(8\eta L) \tag{1}$$
Where the tube's radius is denoted by r, the pressure drop between two terminals of the tube is denoted by Δp, the fluid viscosity coefficient is denoted by η, and the length of the tube is denoted by L. R is conversely correlated with the quartic of the tube diameter ($R=8\eta L/\pi r^4$), that means the resistance is conversely correlated with the quadratic of the minimum airway CSA ($R \propto CSA^{-2}$).

According to Bernoulli Obstruction Theory[33,34], the upper airway resistance is conversely correlated with the minimum airspace CSA ($R \propto CSA^{-1}$), meaning that a 4-fold drop in CSA could lead to a 4-fold rise in the resistance of the upper airway. The Bernoulli equation for steady frictionless incompressible flow and the continuity equation suggests that:
$$Q=A_1V_1=A_2V_2 \tag{2}$$

$$Q = C_D A \sqrt{\frac{2\Delta p}{\rho |1-\beta^4|}} \tag{3}$$

where A is CSA at the constriction, V is air velocity, $\rho = 1.225$ kg/m³ is the density of air. C_D is a function of the geometry (ratio β) and the Reynolds number (Re), and experimental measurements were used to determine its value. The numbers 1 and 2 denote two distinct locations along the airflow streamline, one located at the upstream of the stenosis area and the other in the middle. On the basis of the above equations, we discovered that the Bernoulli Obstruction Theory implies a negative correlation between the upper airway resistance and the obstructed airspace minimum CSA under the limitation of severe obstruction, that is:

$$R_{Total} = R_{Stenosis} = \frac{1}{C_D} \sqrt{\frac{\rho\Delta p}{2}} \frac{1}{A} \quad \text{(severe constriction)} \tag{4}$$

The equation (4) was simplified by assuming severe constricted conditions (β → 0), resulting in $lim_{\beta \to 0}(1 - \beta^4) = 1$. Assuming that the coefficient C_D is relatively constant throughout the pharynx in diverse individuals, this equation implies that the resistance of the pharyngeal is conversely correlated with the airway minimal CSA (R ∝ CSA^{-1}). This equation (5) is a power law utilized to fit the correlation between the airspace minimum CSA and airway resistance in order to test this hypothesis, namely:

$$R = a(CSA)^b \tag{5}$$

where a and b are fitting constants.

2.5. Particle Transport Simulations

The Solution mode's Lagrangian discrete phase model (DPM) of ANSYS FLUENT 2021 R1 follows the Euler‐Lagrange approach. A continuum phase was applied to the fluid phase in this study. ICS particles were assumed as spherical shapes with a unit density (1,000 kg/m³). Simulated ICS particles were released evenly and passively from a planer cross-section at the face mask inlet, and the particle diameters ranged from 1 to 20 μm with 1 μm incrementation. Due to the dilute nature of the particle flow (the particle's volume fraction < 0.1%), the interaction between particles is neglected, and one-way coupling between the airflow fields and the particles is assumed.

The definition of particle DF is the ratio of the particles deposited in an anatomic site to the total number of particles entering the entire model. The particles that reached beneath the target area were considered to enter the lower airway (trachea and lung), and the particles deposited on the target area and above were considered to deposit in the upper airway.

Fluent's DPM mode was applied to follow ICS particles once they were introduced into the mouth, the tracking was ended till the particles were "trapped" by the airway mucosa or particles outflew the upper airway. Since the mucus layer covers the surface of the airway, particle deposition was thought to occur when it hit the airway surface, hence rebounding was not taken into account. Results of particle deposition were subsequently exported as coordinate positions of deposition for further analysis. The subglottis and glottis are collectively referred to as the "targeted area" in this article, and the particles with the highest DF in this area were considered particles with ideal particle sizes.

3.   Results:

3.1. Model validation

Preliminary particle deposition model validation analyses were carried out by releasing particles

with sizes ranging from 1 to 20 μm into the oral-pharynx model. For a comprehensive consideration of the varied inhalation flow rates and diverse particle sizes, the impaction parameter ($I=d_{ae}^2Q$) was introduced here to collapse the series of results into one data set, in which d_{ae}^2 is the diameter of the aerodynamic particle, Q (cm^3/s or L/min) is the inhalation flow rate, and then the results were compared against experimental results from the previous researches. Fig. 4A indicates that the predicted upper airway DF presents an S-shaped curve, and the outcomes of our simulation highly coincide with the in vivo measurement studies of Lippmann, M. et al. [41] Stahlhofen, W. et al.[42] and the CFD model studies of Yousefi M et al.[43], Zhou et al[44]. However, due to anatomical differences and varied inspiratory flow rates to maintain a resting state between children and adults, the pediatric upper airway DF is higher when the inertia parameter is over 10,000 μm^{2}L/min. Fig. 4B compared the upper airway resistances between our mouth-throat model (aged 3- to 5-year-old) and previous nose-throat models[34] (containing 19-month-old, 38-month-old, 93-month-old, and adult models). Our results are basically in accordance with the previous CFD simulations, variation might exist due to the following reasons: 1) children are in the growth and development stage, and their body anatomy undergoes drastic changes every year; 2) the models breathing via mouths in our study might be a bit different from those breathing via noses in the previous study.

3.2. Airway Resistance

In three healthy children's models and 12 croup models with simulated SGS created by virtual 5mm-long spindle-shaped obstructions, the airway resistance was depicted as a function of subglottis minimum airspace CSA. We fitted the CFD findings with a power law curve to examine the association between the minimal CSA at the subglottis and airway resistance.

Our fitting equation is as follows:

$$R = a(CSA)^b$$

where a and b are constants: a=0.06, b=-1.07, |r|=0.97. (Fig. 5) The results demonstrated that airway resistance is negatively correlated with CSA at the subglottis ($R_{TOTAL} \propto CSA^{-1}$), which is in accordance with the Bernoulli Obstruction Theory.

The pressure gradient from the mouth to the trachea progressively rose in the healthy pediatric upper airway models, while the croup models showed a more abrupt rise in pressure developing around the glottis. As the stenosis getting worsen, the resistance of the target area made up an increasing percentage of the overall upper airway resistance. To be more specific, there was an increase in the ratio of the obstruction resistance to the entire upper airway resistance (average± standard deviation) from 12.21%±8.14% in the base models, to 21.39%±5.19% in mild croup models (30%AO), 53.72%±9.29% in moderate croup models (50%AO), 79.41%±9.29% in severe croup models (70%AO). Therefore, as the stenosis grew more and more severe, the pediatric upper airway pressure drop was getting progressively more restricted to the obstruction site at our target area, validating our assumption that, at the limitation of extremely severe stenosis, the stenosis's resistance is noticeably more prominent than the resistance of upstream.

We plotted the graph to illustrate the detailed correlation between the severity of croup and the pressure drop of the upper airway (ΔP) (Fig. 6), and found that only after 70% or more airway lumen was obstructed did ΔP start to rise substantially and sharply. Under the resting state, the average ΔP of our models increased from 25 Pa for the base models to, respectively, 33, 40, and 77 Pa for 30%, 50%, and 70%AO.

3.3. Airflow streamlines

The effects of SGS on laryngeal airflow streamlines are depicted in Fig. 7. From the model of the healthy child (Fig. 7A), moderately distributed velocities and equally distributed airflow streamlines can be observed, and the highest airflow velocity occurs from supraglottic to subglottic areas. The mainstream airflow turned directly into the pharynx after passing through the oral cavity. Cast whirling airflow formed when the airflow impacted the posterior pharyngeal wall, and more vortices were generated in the hypopharynx. The dramatically decreased airway diameter in the glottis and subglottis led to an abrupt acceleration of airflow, and the airflow was relatively flat and straight, with few vortices to be observed.

The overall direction and course of the airflow streamline above the target area were nearly the same in healthy children's models and models with various degrees of the crop, proving that stenosis had little effect on the airflow above the stenosis area. Compared to the base model, in the croup models, the airstream instantly transformed to an extremely speedy airflow while entering the glottis and subglottis region before progressively decelerating within the trachea. Moreover, it was observed that inferior to the obstructed area the airflow seemed to be whirling massively, and the more severe the stenosis is, the more severe the swirling flow becomes.

3.4. Ideal ICS particle size for croup

In the base model, smaller ICS particle sizes (1-5μm) were more likely to escape into the trachea and lungs (DF＞90%), medium ICS particles (6-15μm) were more dispersed throughout the airway, while larger ICS particles (16-20 μm) were expected to be trapped and deposit above the hypopharynx (oral cavity, nasopharynx, oropharynx, etc) (DF ＞70%). The ICS particle deposition patterns of the inhaled particles in varied sizes were shown in Fig. 8. The 3rd quartile (Q3), also referred to as the 75th percentile, was employed to demonstrate effective deposition. The target area DF of no less than seventy-five percent of the maximum DF was assumed as effective deposition. For target drug delivery aiming the base models' simulated target area, the effective ICS particle diameters ranged between 8 to 10 μm. A maximum average DF in the target area of 4.63% was at 8 μm size. (See Fig. 9)

The average target area DF in the mild croup models was lower than that in the base models, while the average target area DFs in the moderate and severe models were greater than that in the base models. In the mild croup models, a maximum DF in the target area of 3.2% was at 8 μm, and the effective deposition particle sizes range from 8 to 10μm. In the moderate croup models, a maximum DF in the target area of 5.36% was at 8 μm, and the effective deposition particle sizes range from 8 to 10 μm. In the severe croup models, a maximum DF in the target area of 12.73% was at 7 μm, and the effective deposition particle sizes range from 6 to 9 μm. Fig. 9 shows the average target area DFs in the base models, mild croup models, moderate croup models, and severe croup models, separately. The intersection of the effective particle sizes of all the models were 8 and 9 μm. Particles produced from traditional nebulizers are predominantly in a range around 1-4 μm, and the average maximum target area DFs within this range was 1.08%, 1.15%, 2.51%, 5.84%, respectively, for healthy children, mild croup children, moderate croup children, and severe croup children.

ICS particle trajectories of different sizes (2μm, 5μm, 8μm, 10μm, 15μm, 20μm) in the base model are shown in Fig. 10. The tendency of particle trajectories was basically consistent with the airflow streamlines. As the ICS particle size gets larger, more and more particles collide on the model surfaces while fewer enter the lower airway. As we can see, when the particle size exceeds 15

355 μm, almost all particle trajectories collide and terminate at the posterior pharyngeal wall while rare can reach below the hypopharynx.

4. Discussion

Croup is a type of respiratory infection that is typically caused by viruses[45]. The infection
360 normally causes spindle-shaped stenosis in the subglottis, which obstructs breathing and causes the characteristic symptoms of a "barking/brassy" cough, stridor, and a hoarse voice. In a straight pipe experiment, Choi.Y et al. [46] examined circular and triangular glottal constriction and demonstrated that the flow pattern completely varied in each case. The airflow field in the upper airway was explored by Brouns et al.[47] and Chen et al. [48] while taking into account glottal folders with
365 various cross-sectional sizes and different shapes. Their findings demonstrate that the glottal aperture's shape and CSA have profound effects on the flow pattern rather than breathing capacity. Therefore, the virtually constructed spindle-shaped stenosis in this study is more precise and closer to the actual clinical condition than ever before. Former studies tended to directly implant a plane to block the airway or utilize cylindrical segments of varying diameters to simulate various degrees of
370 SGS, which was detached from the actual clinical situation and might result in an altered airflow field in the upper airway. Based on the Myer-Cotton classification system, we modeled mild croup with 30%AO, moderate croup with 50% AO, and severe croup with 70%AO. The obstruction area over 70% was not simulated because at that time, the patients' lives were under emergency, and much more effective methods such as tracheotomy may be required. Though this study mainly
375 focused on the glottis area and subglottis area, each of our upper airway models was divided into 14 parts according to the anatomical structures, which is not only anatomically accurate and can display the whole upper airway clear at a glance, but also serves as an aerosolized medication deposition CFD database in the pediatric upper airway which may facilitate further study of inhaled pollution deposition and drug delivery in other anatomical sites.

380 Given that the symptoms of many croup children experience an abrupt onset and progression, a prompt and reliable approach to assess the degree of airway restriction would be instrumental in guiding therapeutic decisions. Additionally, according to our research, the upper airways flow-pressure correlation of children with croup could be appropriately described by the Bernoulli Obstruction Theory, which claims that airway resistance and airway minimum CSA show a negative
385 correlation ($R \propto A^{-1}$), can explain the flow-pressure relationship of the upper airway in children with croup. The inapplicability of the Hagen-Poiseuille equation here may because this equation is only valid in fully-developed, laminar flow in straight circular tubes, while the laminar-transitional-turbulent airflow in the human upper airway, the entrance effects as well as the curving structure combined to invalidate this assumption. In constricted upper airway models, the
390 majority of the pressure drop of the total upper airway is generated by the constriction (Fig. 6). As a result, even slight changes in the minimal CSA would exert a substantial impact on the upper airway resistance, and R and minimum CSA show a strong connection (Fig. 5). Contrarily, a more uniform distribution of resistance can be observed along the upper airway in models with less severe constrictions and healthy pediatric models.

395 In the current work, pressure drops across the upper airway with various constrictions in realistic upper airways was examined. The findings predicted, in keeping with what is witnessed in clinical practice, that once the stenosis has progressed to a rather severe degree, patients will experience a relatively dramatic and immediate surge in respiratory distress. The pediatric upper

airway models' (between mouths and the end of subglottis) pressure-flow relationship showed a power law relationship, that the simulated $\varDelta P$ began to surge drastically only until no less than 70% of the upper airway lumen was obstructed, which is in accordance with the study of Brouns et al. that focused on the tracheal stenosis[49]. The average $\varDelta P$ of our models rose from 25 Pa for the base models to 33, 40, and 77 Pa for 30%, 50%, and 70% stenosis, respectively. This finding is consistent with the research showing that individuals with tracheal stenosis typically experience a surprisingly instant onset of dyspnea, which can typically be observed at the period of clinic admission when there has been a loss of no less than 75% of the airway lumen[50]. Together, these results demonstrated that, while there obviously was time for airway stenosis to progress progressively before the patient experiences clinically significant breathing impairment, however, once the severity of stenosis exceeded a specific degree, the upper airway pressure drop ($\varDelta P$) abruptly got serious and the dyspneic respiration developed instantly, and intervention should be carried out in an emergency situation. The degree of laryngeal obstruction in the croup is divided according to the patients' clinical manifestation, while objective methods to gauge the seriousness of obstruction and the prediction of therapeutic responses remain absent. The close relationship between airway CSA and airway resistance, and its consistency with clinical manifestation may suggest that the degree of airway obstruction in croup can be assessed by calculating the AO% under the laryngoscope. When the AO% exceeds 70%, early aggressive therapy such as intravenous injection of glucocorticoids as well as sedatives may be indispensable, and may even turn to tracheotomy if all the conservative treatments failed.

Typically, a single oral dosage of steroids is prescribed to treat croup[45,51]. To imitate the realistic treatment procedure, models of children with nebulizer masks attached to their faces were constructed to simulate the actual treatment process. Our study employed CFPD methodology to find out the ideal ICS particle sizes for topical target area (glottis+subglottis) deposition in healthy children's upper airway models and children with mild, moderate, and severe croup. Based on numerical simulations, we spotted that the moderate and severe croup (more than 50% AO) generally facilitated localized target area DF of the inhaled particles, while the mild croup (30% AO) reduced localized target area DF.

Since the inhalation flow rate is at a low to moderate level in resting conditions, the related airflow field is typically believed to be laminar flow across the majority of the upper airway area. However, for limiting regions of airflow, such as the glottis, flow velocity accelerates to become transitional and turbulent flow due to significantly narrowed passage space, and the glottis's narrow CSA will result in great turbulent kinetic energy[48]. The turbulence intensity and the shear stress are both amplified by the high velocity gradient produced by the small CSA. In the trachea, the geometric model with the larger glottis exhibits fewer vortices than the model with the smaller glottis[48]. Our results were consistent with these earlier interpretations. In our study, compared to the base model, in the croup models, the airstream instantaneously converted to an extremely rapid flow in the glottis before progressively decelerating within the trachea and the airflow was seen to be whirling below the obstructed area. Moreover, the intensity of the whirling flow increases with the severity of the stenosis, which is also the same as the study of Chen et al[48]. Airflow vortices lead to particle deposition by impacting the airway mucous, which may explain why the target area DFs of the inhaled particles in moderate and severe croup models were greater than that in the healthy models. But why the target area DFs in the mild croup models were lower than that in the healthy models? The narrowest portion of the laryngopharynx is the glottis, where the vocal cord is attached.

The mild croup (30%AO) narrowed the subglottis to be as wide as the glottis, which means the target area becomes a cylinder with constant width. The inhomogeneity of the incoming flow velocity is the primary cause of turbulence, therefore cylinders with constant-width lead to fewer vortexes inside this area. The onset of turbulence and laryngeal jet are the main reasons for this high deposition rate in the large segments, inertial impaction is the dominant deposition mechanism[52,53], and these combined to result in high DF in the croup model target areas.

Since oral aerosol deposition is far less than that in the nasal passages, aerosol medications are typically administered to the larynx and lower airway by inhalation via the oral passages, so that more drugs can reach the lesion location. In all of the models, the maximum target area DF can be achieved when the ICS particle sizes range over 7-8μm. As shown in Fig. 8, the intersection of the effective particle sizes of all the models are 8 and 9 μm, meaning that at this time, the aerosol therapy is most effective for all croup severity. The particle sizes that are released by the routinely prescribed inhalers (1-4 μm) were aimed at the tracheobronchial and alveolar-interstitial region[20], which are smaller than the ideal sizes we predicted based on our models, and the maximum target area DFs of these commercially available nebulizers are awfully small. These findings suggest that the available nebulizers may be not suitable for croup treatment in pediatrics, inhalers with larger ICS particles are needed to improve the curative effect. Even if our results are preliminary, they are persuasive and demand further research. These discoveries can contribute to our understanding of the dynamic nature of the human airway and may potentially lead to the creation of innovative inhalers that release particles specifically suited for therapeutic laryngeal administration.

In this study, a simplification, steady-state condition was identified as a solid approximation for the brief single-cycle inspiratory duration. Our previous studies and numerous investigations have concluded and tested that under resting breathing conditions, the nasal airflow can be considered quasi-steady flow [54,55]. Experimental evidence demonstrates that oscillatory effects do not appear until Womersley numbers (α) are higher than 4 [56]. It was also determined that a Strouhal number (St) $\leqslant$ 0.2 was an appropriate criterion when the differences between solutions of the unsteady and steady flow field can be neglected, and the assumption of steady airflow was reasonable under these conditions [57-59]. For the glottis region in present study, the Strouhal number was calculated as: $St=fd/U$, where U is the average airflow velocity through the subglottis plane, d is the hydraulic diameter of the subglottis plane, and f is the respiratory frequency in Hz. Womersley number was calculated as: $\alpha=d/2*(2\pi f/v_g)$, where v_g denotes the kinematic viscosity of air. In this study, the d was 7.64mm, 6.86 mm, and 7.23mm, and U was 3.317m/s, 3.51m/s, and 3.53m/s for the three children accordingly. The calculated St numbers were 8.5×10^{-4}, 7.2×10^{-4}, and 7.6×10^{-4}, and the calculated α numbers were 1.38, 1.23, and 1.30, respectively. Therefore, based on calculated Strouhal and Womersley numbers, it can be concluded that all case studies considered in this paper satisfy the criterion for quasi-steady flow. Although the quasi-steady airflow assumption can reasonably reflect the airflow characteristics in examined airways, the instantaneous deposition of microparticles because of unsteady accelerating and decelerating flow is ignored in the present study. Nevertheless, neglecting the instantaneous deposition features is an approximation that is used in the present analysis, which may be considered as a limitation of our research and can be addressed in future studies.

The considerably small cohort analyzed in this study is inevitably one of our limitations,

11

and the stenosis was virtually constructed based on the healthy model rather than the CT from the actual children with croup. This is because laryngoscopy is the preferred approach for diagnosing croup, and CT scanning is not typically performed on children. Second, though we validated our model predictions with the outcome of experimental measurements and simulations, part of the presented comparative data refers to adults and nose-throat models. This is because though there are several numerical estimates in the published literature focusing on the quantification of deposition in pediatric airways, virtually no one focus on the glottis area or subglottis area. Third, the particles were also not presumed to interact with one another, modify the inhalational airflow, or re-enter the airflow after impacting the boundary of the airway. Fourth, even though CFPD studies utilizing geometries based on CT have been confirmed to be faithful and valid as ways to forecast particle delivery and airflow, all these techniques can only generate simulations in static, while the airway is dynamic[60,61]. Finally, in vivo validation was not performed in this study, making it a purely computational investigation. In vitro and in vivo experiments need to be carried out in the future as a way to support or contradict our theories.

5. Conclusions

In this study, CFPD modeling of pediatric upper airway airflow, inhalation drug delivery, and airway resistance in healthy children and children with various degrees of croup was performed to understand the underlying particle transport and deposition mechanism. The results showed that the resistance of the pediatric upper airway is conversely proportional to airway minimum CSA ($R \propto CSA^{-1}$), and when the constriction of the subglottis reaches a certain value ($\geq 70\%$ obstruction), the upper airway pressure drop abruptly surged and the dyspneic respiration symptoms of patients develop instantly. Moreover, in all considered models, the maximum target area DF can be reached when the ICS particle sizes are 7 or 8 μm, all models can achieve effective target area delivery when the ICS particles size are 8 and 9 μm, whereas almost all commercial and medical nebulizers produce smaller particles (1-4μm) than what we suggested. These may provide guidance for the evaluation of the croup severity, and promisingly, may help develop novel nebulizers, especially for pediatric targeting the glottis and subglottis so as to achieve superior croup curative effect.

CRediT authorship contribution statement
Yusheng Wang: Conceptualization, Data curation, Formal analysis, Software, Methodology, Validation, Formal analysis, Writing—original draft, Writing - review & editing; **Ruiping Ma:** Term, Data curation; **Siping Sun:** Conceptualization, Methodology; **Zhenzhen Hu:** Investigation, Visualization; **Chaofan Li:** Data Curation, Validation; **Miao Lou:** Software, ; **Minjie Gong:** Supervision, Visualization; **Zhenbo Tong:** Methodology, Writing—review and editing; **Feilun Yang:** Validation; **Jingguo Chen:** Conceptualization; **Guoxi Zheng:** Formal analysis, Writing—review and editing, Funding acquisition; **Jingliang Dong:** Supervision Methodology, Funding acquisition, Writing—review and editing; **Ya Zhang:** Funding acquisition, Project administration, Resources, Conceptualization, Methodology, Formal analysis, Writing—review and editing, . All authors have read and agreed to the published version of the manuscript.

82000960); the Universities Co-Funded Project of Key Research and Development Project of Shaanxi Province (grant number 2020GXLH-Y-017); the Science and Technology Planning Project of Yulin City (grant number CXY-2020-047); and the Australian Research Council (grant number DE210101549).

References

[1].Bjornson CL, Johnson DW. Croup. *The Lancet* 2008; **371**(9609): 329-39.https://doi.org/10.1016/S0140-6736(08)60170-1.

[2].Everard ML. Acute bronchiolitis and croup. *Pediatr Clin North Am* 2009; **56**(1): 119-33, x-xi.10.1016/j.pcl.2008.10.007.

[3].Johnson D. Croup. *BMJ Clin Evid* 2009; **2009**.

[4].Hodnett BL, Simons JP, Riera KM, Mehta DK, Maguire RC. Objective endoscopic findings in patients with recurrent croup: 10-year retrospective analysis. *Int J Pediatr Otorhinolaryngol* 2015; **79**(12): 2343-7.10.1016/j.ijporl.2015.10.039.

[5].Hiebert JC, Zhao YD, Willis EB. Bronchoscopy findings in recurrent croup: A systematic review and meta-analysis. *Int J Pediatr Otorhinolaryngol* 2016; **90**: 86-90.10.1016/j.ijporl.2016.09.003.

[6].Cherry JD. Clinical practice. Croup. *N Engl J Med* 2008; **358**(4): 384-91.10.1056/NEJMcp072022.

[7].Russell K, Wiebe N, Saenz A, et al. Glucocorticoids for croup. *Cochrane Database Syst Rev* 2004; (1): Cd001955.10.1002/14651858.CD001955.pub2.

[8].Bjornson CL, Johnson DW. Croup-Treatment Update. *Pediatric Emergency Care* 2005; **21**(12).

[9].Fitzgerald DA. The assessment and management of croup. *Paediatr Respir Rev* 2006; **7**(1): 73-81.10.1016/j.prrv.2005.09.002.

[10].Rittichier KK. The role of corticosteroids in the treatment of croup. *Treat Respir Med* 2004; **3**(3): 139-45.10.2165/00151829-200403030-00002.

[11].Tibballs J, Shann FA, Landau LI. Placebo-controlled trial of prednisolone in children intubated for croup. *Lancet* 1992; **340**(8822): 745-8.10.1016/0140-6736(92)92293-o.

[12].Kuusela AL, Vesikari T. A randomized double-blind, placebo-controlled trial of dexamethasone and racemic epinephrine in the treatment of croup. *Acta Paediatr Scand* 1988; **77**(1):

575   99-104.10.1111/j.1651-2227.1988.tb10606.x.

[13].Husby S, Agertoft L, Mortensen S, Pedersen S. Treatment of croup with nebulised steroid (budesonide): a double blind, placebo controlled study. *Arch Dis Child* 1993; **68**(3): 352-5.10.1136/adc.68.3.352.

[14].Huang T, Xia ZF, Li WQ. Efficacy of inhaled budesonide on serum inflammatory factors and quality of
580   life among children with acute infectious laryngitis. *Am J Otolaryngol* 2021; **42**(1): 102820.10.1016/j.amjoto.2020.102820.

[15].Ellul‐Micallef R, Johansson S. Acute dose‐response studies in bronchial asthma with a new corticosteroid, budesonide. *British journal of clinical pharmacology* 1983; **15**(4): 419-22.

[16].Khilnani G, Banga A. Non-invasive ventilation in chronic obstructive pulmonary. *Medicine (Baltimore)*
585   2008; **18**.

[17].El Taoum KK, Xi J, Kim J, Berlinski A. In Vitro Evaluation of Aerosols Delivered via the Nasal Route. *Respir Care* 2015; **60**(7): 1015-25.10.4187/respcare.03606.

[18].Sommerfeld M, Cui Y, Schmalfuß S. Potential and constraints for the application of CFD combined with Lagrangian particle tracking to dry powder inhalers. *Eur J Pharm Sci* 2019; **128**:
590   299-324.10.1016/j.ejps.2018.12.008.

[19].Kadota K, Matsumoto K, Uchiyama H, et al. In silico evaluation of particle transport and deposition in the airways of individual patients with chronic obstructive pulmonary disease. *European Journal of Pharmaceutics and Biopharmaceutics* 2022; **174**: 10-9.https://doi.org/10.1016/j.ejpb.2022.03.010.

[20].Chalvatzaki E, Chatoutsidou SE, Lazaridis M. Simulations of the deposition of pharmaceutical
595   aerosols in the human respiratory tract by dry powder inhalers (DPIs). *Journal of Drug Delivery Science and Technology* 2020; **59**: 101915.https://doi.org/10.1016/j.jddst.2020.101915.

[21].Ahookhosh K, Saidi M, Mohammadpourfard M, et al. Flow Structure and Particle Deposition Analyses for Optimization of a Pressurized Metered Dose Inhaler (pMDI) in a Model of Tracheobronchial Airway. *Eur J Pharm Sci* 2021; **164**: 105911.10.1016/j.ejps.2021.105911.

600   [22].Darquenne C. Aerosol deposition in health and disease. *J Aerosol Med Pulm Drug Deliv* 2012; **25**(3): 140-7.10.1089/jamp.2011.0916.

[23].Rahman MM, Zhao M, Islam MS, Dong K, Saha SC. Aging effects on airflow distribution and micron-particle transport and deposition in a human lung using CFD-DPM approach. *Advanced Powder Technology* 2021; **32**(10): 3506-16.https://doi.org/10.1016/j.apt.2021.08.003.

605   [24].Dong J, Shang Y, Inthavong K, Chan HK, Tu J. Numerical Comparison of Nasal Aerosol Administration Systems for Efficient Nose-to-Brain Drug Delivery. *Pharm Res* 2017; **35**(1): 5.10.1007/s11095-017-2280-6.

[25].Sun Q, Dong J, Zhang Y, Tian L, Tu J. Numerical study of the effect of nasopharynx airway obstruction on the transport and deposition of nanoparticles in nasal airways. *Experimental and Computational Multiphase Flow* 2022; **4**(4): 399-408.10.1007/s42757-022-0143-9.

610   [26].Perkins EL, Basu S, Garcia GJM, Buckmire RA, Shah RN, Kimbell JS. Ideal Particle Sizes for Inhaled Steroids Targeting Vocal Granulomas: Preliminary Study Using Computational Fluid Dynamics. *Otolaryngol Head Neck Surg* 2018; **158**(3): 511-9.10.1177/0194599817742126.

[27].Gosman RE, Sicard RM, Cohen SM, Frank-Ito DO. Comparison of Inhaled Drug Delivery in Patients With One- and Two-level Laryngotracheal Stenosis. *Laryngoscope* 2022: 10.1002/lary.30212.

615   [28].Wang J, Zhang Y, Chen X, et al. Targeted delivery of inhalable drug particles in the tracheobronchial tree model of a pediatric patient with bronchopneumonia: A numerical study. *Respiratory Physiology & Neurobiology* 2023; **311**: 104024.https://doi.org/10.1016/j.resp.2023.104024.

[29].Amirav I, Newhouse MT. Deposition of small particles in the developing lung. *Paediatr Respir Rev*

2012; **13**(2): 73-8.10.1016/j.prrv.2011.05.006.

620 [30].Fitzgerald DA, Kilham HA. Croup: assessment and evidence‑based management. *Medical journal of Australia* 2003; **179**(7): 372-7.

[31].Myer CM, O'Connor DM, Cotton RT. Proposed Grading System for Subglottic Stenosis Based on Endotracheal Tube Sizes. *Annals of Otology, Rhinology & Laryngology* 1994; **103**(4): 319-23.10.1177/000348949410300410.

625 [32].Hartnick C, Cotton R. Stridor and airway obstruction. *Pediatric Otolaryngology* 2002; **4**: 1437-47.

[33].Garcia GJM, Hariri BM, Patel RG, Rhee JS. The relationship between nasal resistance to airflow and the airspace minimal cross-sectional area. *J Biomech* 2016; **49**(9): 1670-8.10.1016/j.jbiomech.2016.03.051.

[34].Lin EL, Bock JM, Zdanski CJ, Kimbell JS, Garcia GJM. Relationship between degree of obstruction and 630 airflow limitation in subglottic stenosis. *Laryngoscope* 2018; **128**(7): 1551-7.10.1002/lary.27006.

[35].Hofmann W. Mathematical model for the postnatal growth of the human lung. *Respir Physiol* 1982; **49**(1): 115-29.10.1016/0034-5687(82)90106-2.

[36].Ghalichi F, Deng X, De Champlain A, Douville Y, King M, Guidoin R. Low Reynolds number turbulence modeling of blood flow in arterial stenoses. *Biorheology* 1998; **35**(4-5): 635 281-94.10.1016/s0006-355x(99)80011-0.

[37].Shang Y, Inthavong K. Numerical assessment of ambient inhaled micron particle deposition in a human nasal cavity. *Experimental and Computational Multiphase Flow* 2019; **1**(2): 109-15.10.1007/s42757-019-0015-0.

[38].Zhang Z, Kleinstreuer C. Low-Reynolds-number turbulent flows in locally constricted conduits: a 640 comparison study. *AIAA journal* 2003; **41**(5): 831-40.

[39].Basu S, Frank-Ito DO, Kimbell JS. On computational fluid dynamics models for sinonasal drug transport: Relevance of nozzle subtraction and nasal vestibular dilation. *Int J Numer Method Biomed Eng* 2018; **34**(4): e2946.10.1002/cnm.2946.

[40].Foitzik B, Schmalisch G, Wauer RR. [Effect of physical properties of respiratory gas on 645 pneumotachographic measurement of ventilation in newborn infants]. *Biomed Tech (Berl)* 1994; **39**(4): 85-92.10.1515/bmte.1994.39.4.85.

[41].Lippmann M, Albert RE. The effect of particle size on the regional deposition of inhaled aerosols in the human respiratory tract. *Am Ind Hyg Assoc J* 1969; **30**(3): 257-75.10.1080/00028896909343120.

[42].Stahlhofen W, Gebhart J, Heyder J. Experimental determination of the regional deposition of aerosol 650 particles in the human respiratory tract. *Am Ind Hyg Assoc J* 1980; **41**(6): 385-98a.10.1080/15298668091424933.

[43].Yousefi M, Inthavong K, Tu J. Effect of Pressurized Metered Dose Inhaler Spray Characteristics and Particle Size Distribution on Drug Delivery Efficiency. *J Aerosol Med Pulm Drug Deliv* 2017; **30**(5): 359-72.10.1089/jamp.2016.1299.

655 [44].Cheng Y-S, Zhou Y, Chen BT. Particle Deposition in a Cast of Human Oral Airways. *Aerosol Science and Technology* 1999; **31**(4): 286-300.10.1080/027868299304165.

[45].Rajapaksa S, Starr M. Croup - assessment and management. *Aust Fam Physician* 2010; **39**(5): 280-2.

[46].Choi Y, Wroblewski DE. Characteristics of glottis-induced turbulence in oscillatory flow: an empirical investigation. *J Biomech Eng* 1998; **120**(2): 217-26.10.1115/1.2798305.

660 [47].Brouns M, Verbanck S, Lacor C. Influence of glottic aperture on the tracheal flow. *J Biomech* 2007; **40**(1): 165-72.10.1016/j.jbiomech.2005.10.033.

[48].Chen W, Wang L, Chen L, Ge H, Cui X. Numerical study of the impact of glottis properties on the

airflow field in the human trachea using V-LES. *Respir Physiol Neurobiol* 2022; **295**: 103784.10.1016/j.resp.2021.103784.

[49].Brouns M, Jayaraju ST, Lacor C, et al. Tracheal stenosis: a flow dynamics study. *J Appl Physiol (1985)* 2007; **102**(3): 1178-84.10.1152/japplphysiol.01063.2006.

[50].Willems L. Interventional Pulmonary Medicine. Lung Biology in Health and Disease. Eur Respiratory Soc; 2005.

[51].Gates A, Gates M, Vandermeer B, et al. Glucocorticoids for croup in children. *Cochrane Database Syst Rev* 2018; **8**(8): Cd001955.10.1002/14651858.CD001955.pub4.

[52].Ahookhosh K, Yaqoubi S, Mohammadpourfard M, Hamishehkar H, Aminfar H. Experimental investigation of aerosol deposition through a realistic respiratory airway replica: An evaluation for MDI and DPI performance. *Int J Pharm* 2019; **566**: 157-72.10.1016/j.ijpharm.2019.05.058.

[53].Ahookhosh K, Saidi M, Aminfar H, Mohammadpourfard M, Hamishehkar H, Yaqoubi S. Dry powder inhaler aerosol deposition in a model of tracheobronchial airways: Validating CFD predictions with in vitro data. *Int J Pharm* 2020; **587**: 119599.10.1016/j.ijpharm.2020.119599.

[54].Wen J, Inthavong K, Tu J, Wang S. Numerical simulations for detailed airflow dynamics in a human nasal cavity. *Respir Physiol Neurobiol* 2008; **161**(2): 125-35.10.1016/j.resp.2008.01.012.

[55].Yan Y, Dong J, Tu J. Comparative modelling of inspiratory airflow and micron particle deposition patterns in monkey and human nasal airways. *Journal of Aerosol Science* 2023; **167**: 106099.

[56].Isabey D, Chang HK. Steady and unsteady pressure-flow relationships in central airways. *J Appl Physiol Respir Environ Exerc Physiol* 1981; **51**(5): 1338-48.10.1152/jappl.1981.51.5.1338.

[57].Shi H, Kleinstreuer C, Zhang Z. Laminar airflow and nanoparticle or vapor deposition in a human nasal cavity model. *J Biomech Eng* 2006; **128**(5): 697-706.10.1115/1.2244574.

[58].Bahmanzadeh H, Abouali O, Faramarzi M, Ahmadi G. Numerical simulation of airflow and micro-particle deposition in human nasal airway pre- and post-virtual sphenoidotomy surgery. *Comput Biol Med* 2015; **61**: 8-18.10.1016/j.compbiomed.2015.03.015.

[59].Krane M, Barry M, Wei T. Unsteady behavior of flow in a scaled-up vocal folds model. *J Acoust Soc Am* 2007; **122**(6): 3659-70.10.1121/1.2409485.

[60].Choi J, Xia G, Tawhai MH, Hoffman EA, Lin CL. Numerical study of high-frequency oscillatory air flow and convective mixing in a CT-based human airway model. *Ann Biomed Eng* 2010; **38**(12): 3550-71.10.1007/s10439-010-0110-7.

[61].Miyawaki S, Tawhai MH, Hoffman EA, Lin CL. Effect of carrier gas properties on aerosol distribution in a CT-based human airway numerical model. *Ann Biomed Eng* 2012; **40**(7): 1495-507.10.1007/s10439-011-0503-2.

Grade (% obstructed)	Age (years)	Gender	Inhalation rate(L/min)	Minimum CSA (cm^2)	Pressure Drop (Pa)
Participant 1					
Healthy (0%)	5	F	9.77	0.49	25.29
Mild crop (30%)				0.34	30.95
Moderate crop (50%)				0.25	48.21
Severe crop (70%)				0.15	74.90
Participant 2					
Healthy (0%)				0.43	27.05

Mild crop (30%)	4	F	9.03	0.30	28.83
Moderate crop (50%)				0.22	41.23
Severe crop (70%)				0.13	75.60
Participant 3					
Healthy (0%)	5	F	9.77	0.46	21.26
Mild crop (30%)				0.32	23.59
Moderate crop (50%)				0.23	33.98
Severe crop (70%)				0.14	80.79

Table 1 Demographics, inhalation rate, airway minimal cross-sectional area (CSA), and pressure drop from the inlet of the face mask to the outlet at steady-state breathing conditions for the models of healthy children and children with croup.

M = male, F = female.

Figure legends

Fig. 1. The three-dimensional (3D) reconstruction model (base model) of a 4-year-old healthy child's upper airway with a nebulization face mask attached to the face. A total of three base models were constructed, while only one was displayed throughout this article for clearance and readability. (left view) (A) The different anatomic sites of the pediatric airway were colored in different colors, and the magnified area in the black frame is our target area (the upper part is the glottis and the lower part is the subglottis). (B) The hexahedral cells with five prism layers of the base model in the sagittal position.

Fig. 2. The flow chart of base model construction and data collection.

Fig. 3. The construction process of virtual croup models. (A) The origin subglottis of the base model was split into two parts based on the mid-line (the straight red dotted line), the left and the right part simultaneously move towards the mid-line. The blue dotted curve denotes the mile croup, the green dotted curve denotes the moderate croup, the orange dotted curve denotes the severe croup, and then each of them was slightly modified to be more realistic. The final virtual mild, moderate and severe croup models are shown in (B), (C), (D), respectively. Figures in the upper row were the top view, and figures in the lower row were the front view.

Fig. 4. (A) Deposited fraction (DF) in the mouth-throat area of adults as a function of the impaction parameter (I), expressed as $d_{ae}^2 Q$ from a series of CFD studies and in vivo measurement studies, and compared with the results in our models. (B) Comparison of upper airway resistances in our oral-pharynx model and previous nose-throat models.

Fig. 5. Airway resistance in simulated croup (stenosis) models and base models as a function of airspace cross-sectional area.

Fig. 6. The relationship between the average pressure drop of the pediatric upper airway (ΔP) and the severity of airway obstruction (left view). (A): healthy child model (base model), (B): mild croup model (30% AO); (C): moderate croup model (50% AO) and (D)severe croup model (70% AO).

17

Fig. 7. Airflow streamline patterns in the upper airway models colored by various velocities in (A): healthy child model (base model), (B): mild croup model (30% AO); (C): moderate croup model (50%AO) and (D)severe croup model (70% AO). The figures in the upper row are in the left view, the figures in the lower row are in the back view.

Fig. 8. Particle deposition pattern in the pediatric upper airways. (A) healthy child (base model), (B) mild croup model (30% AO); (C) moderate croup model (50% AO) and (D) severe croup model (70% AO). ICS particles of different sizes are shown in different colors. The figures in the left row with face masks are in the left view, the figures in the right row without face masks are in the left rear view.

Fig. 9. The average target area deposited efficiency of ICS particles ranging between 1 to 20 µm in base models and croup models. The shaded area manifests the effective deposition (DF>75% of maximum deposition). The red line shows the overlapped particle size for all considered upper airway models (8 and 9 µm).

Fig. 10. ICS particle trajectories of different sizes in the base model, the figures in the upper row are the left view and the bottom row are the back view. Different particle velocities are displayed in different colors.
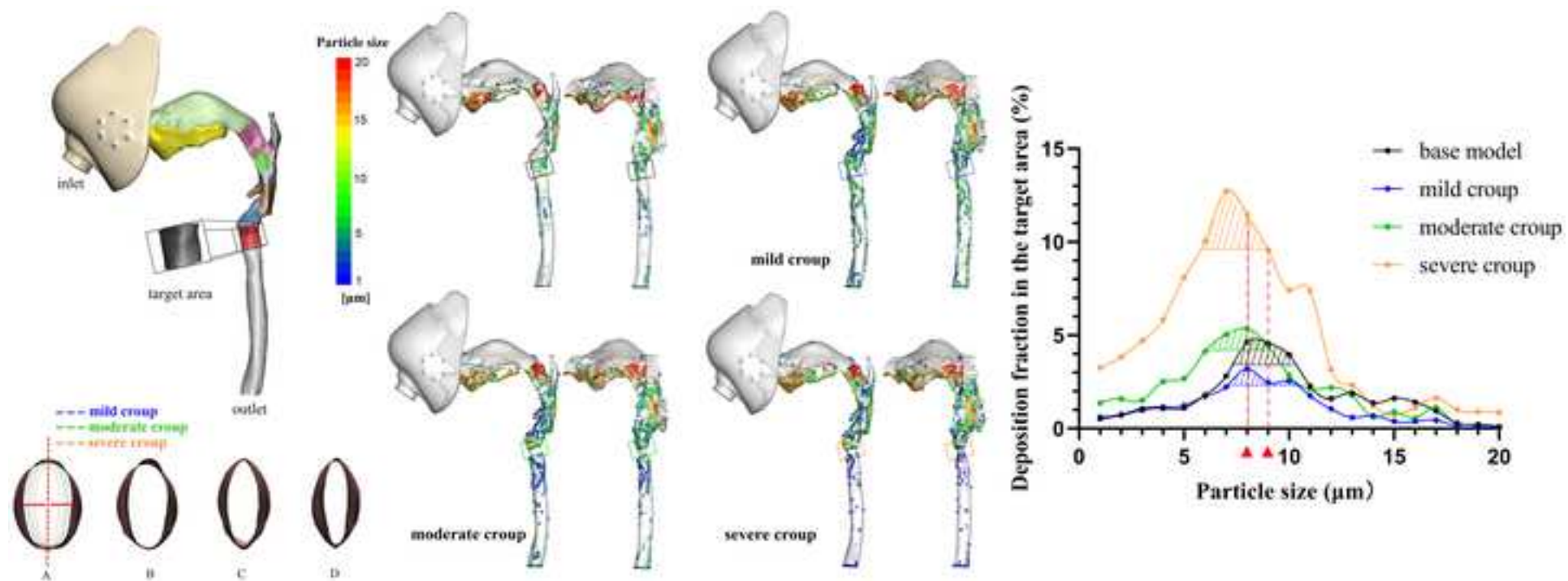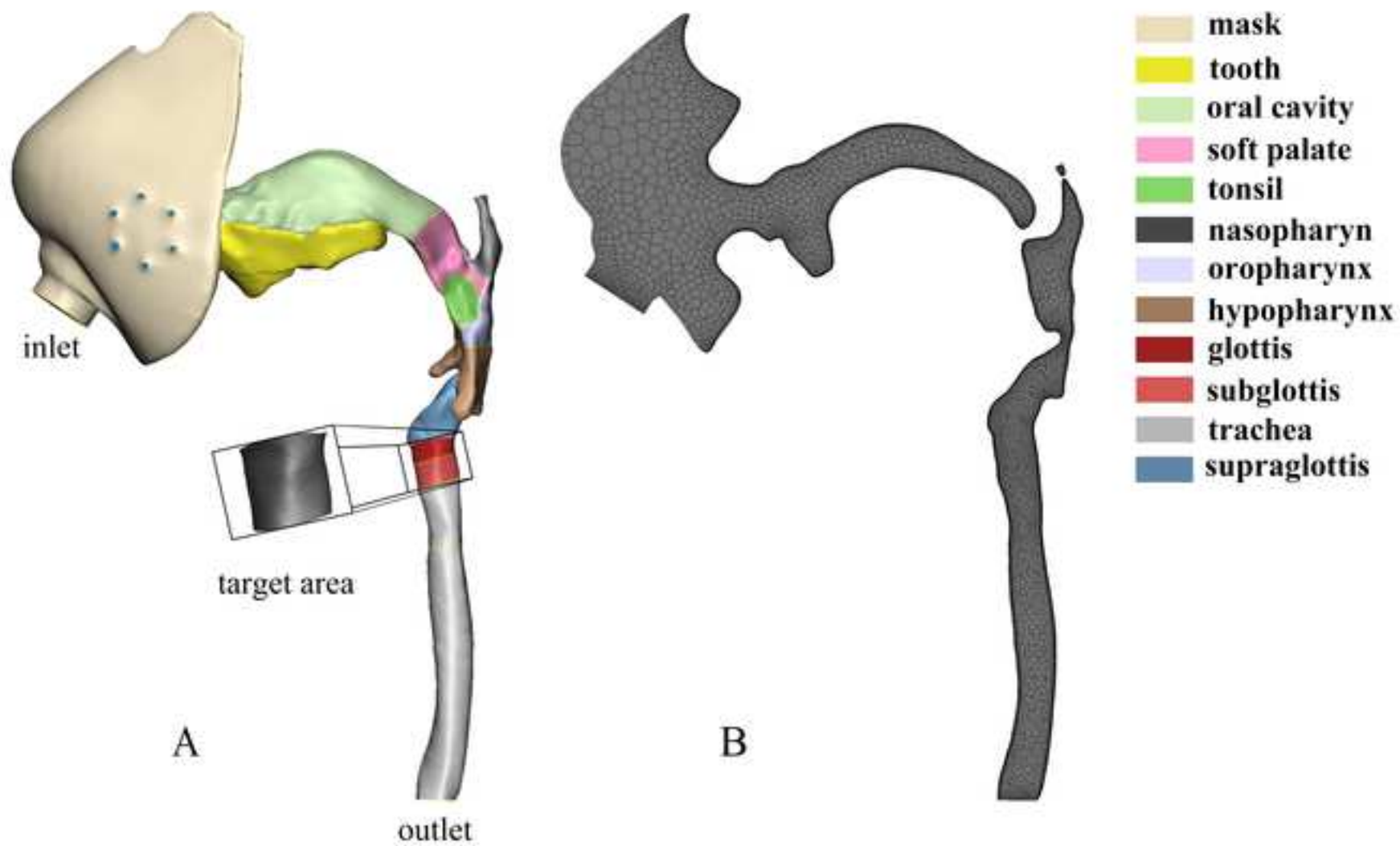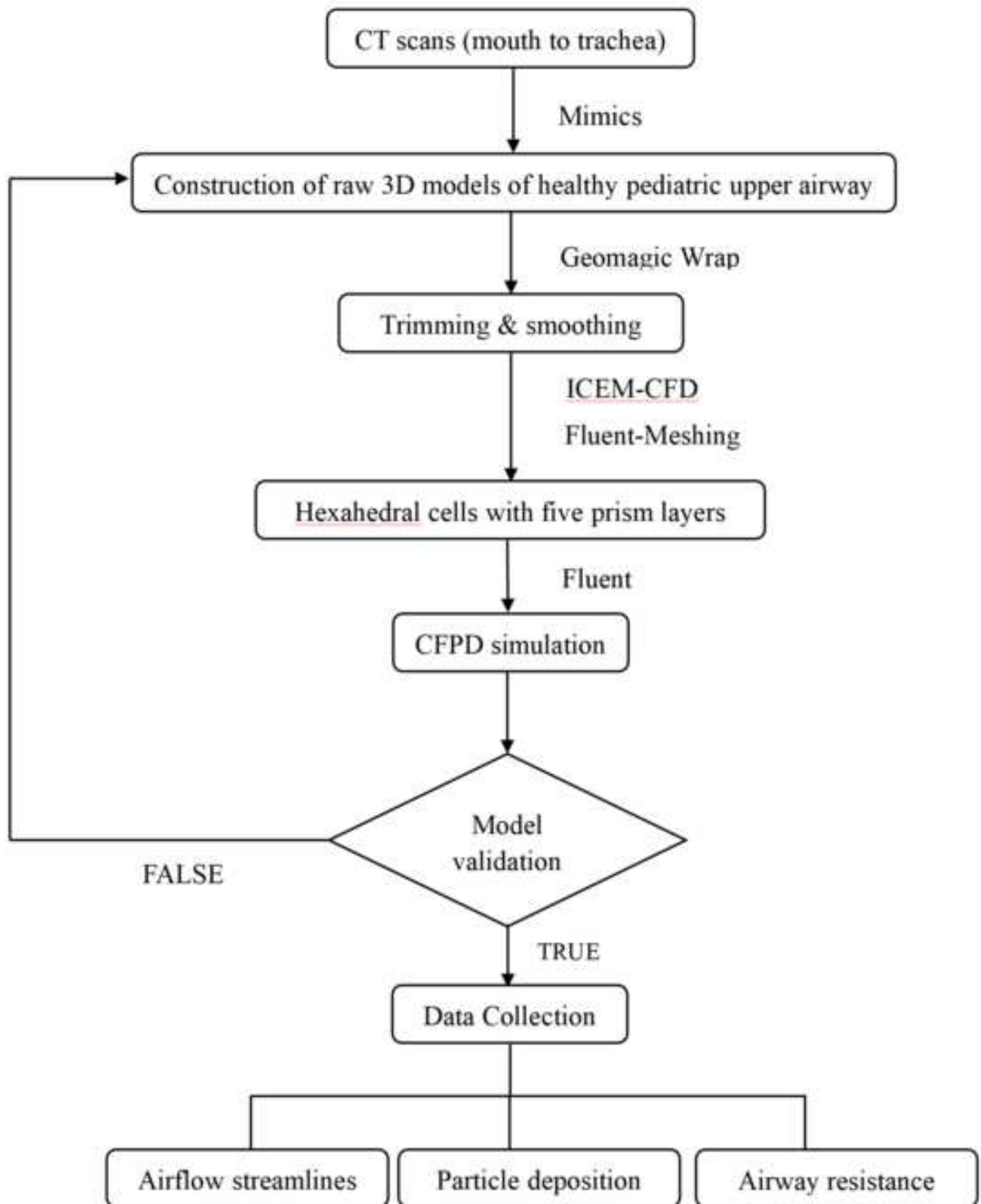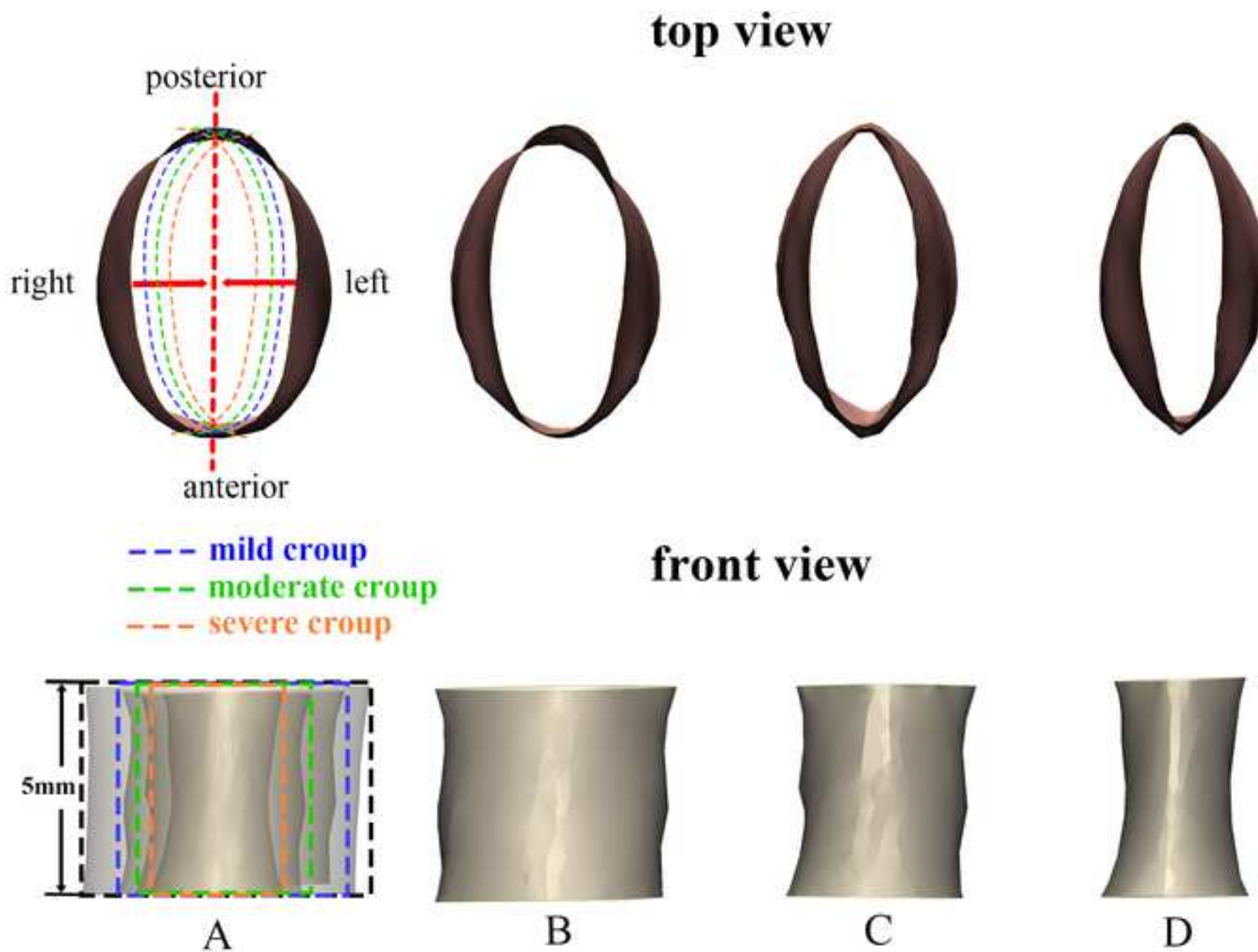
Figure 1

Click here to access/download;Figure;Figure 1.jpg

inlet

target area

outlet

A

B

mask
tooth
oral cavity
soft palate
tonsil
nasopharyn
oropharynx
hypopharynx
glottis
subglottis
trachea
supraglottis

Figure 2

Figure 3

top view

posterior

right

left

anterior

- - - mild croup
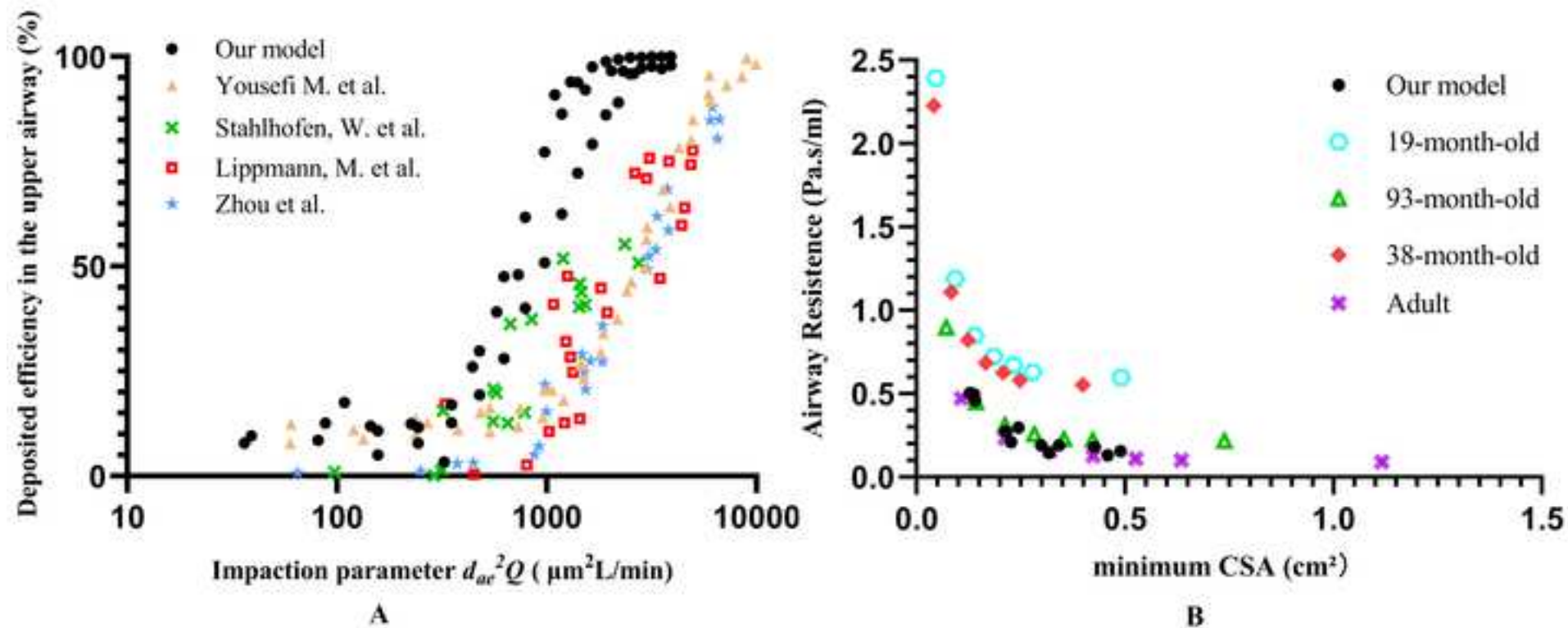- - - moderate croup
- - - severe croup

front view

5mm

A

B

C

D

Figure 4

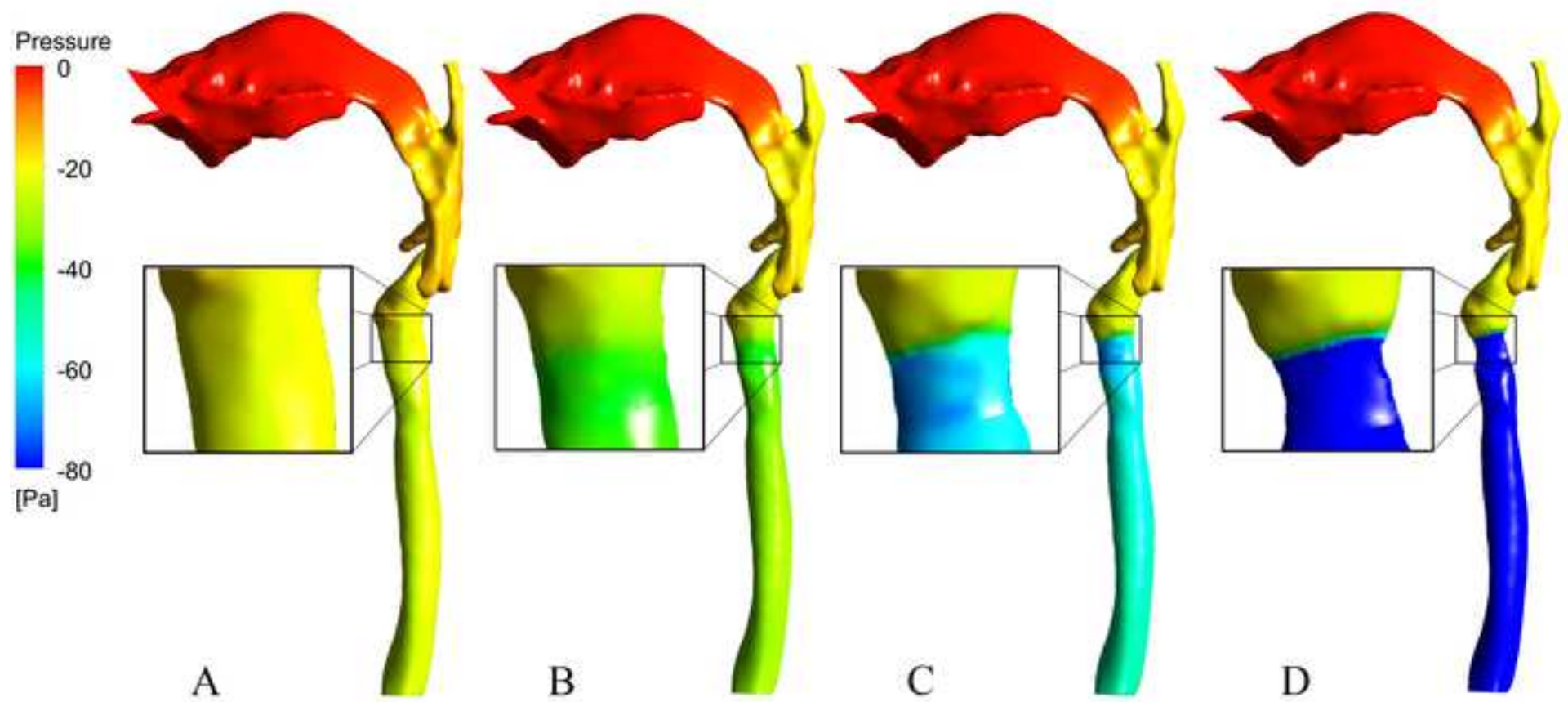Click here to access/download;Figure;Figure 4.tif ⬇
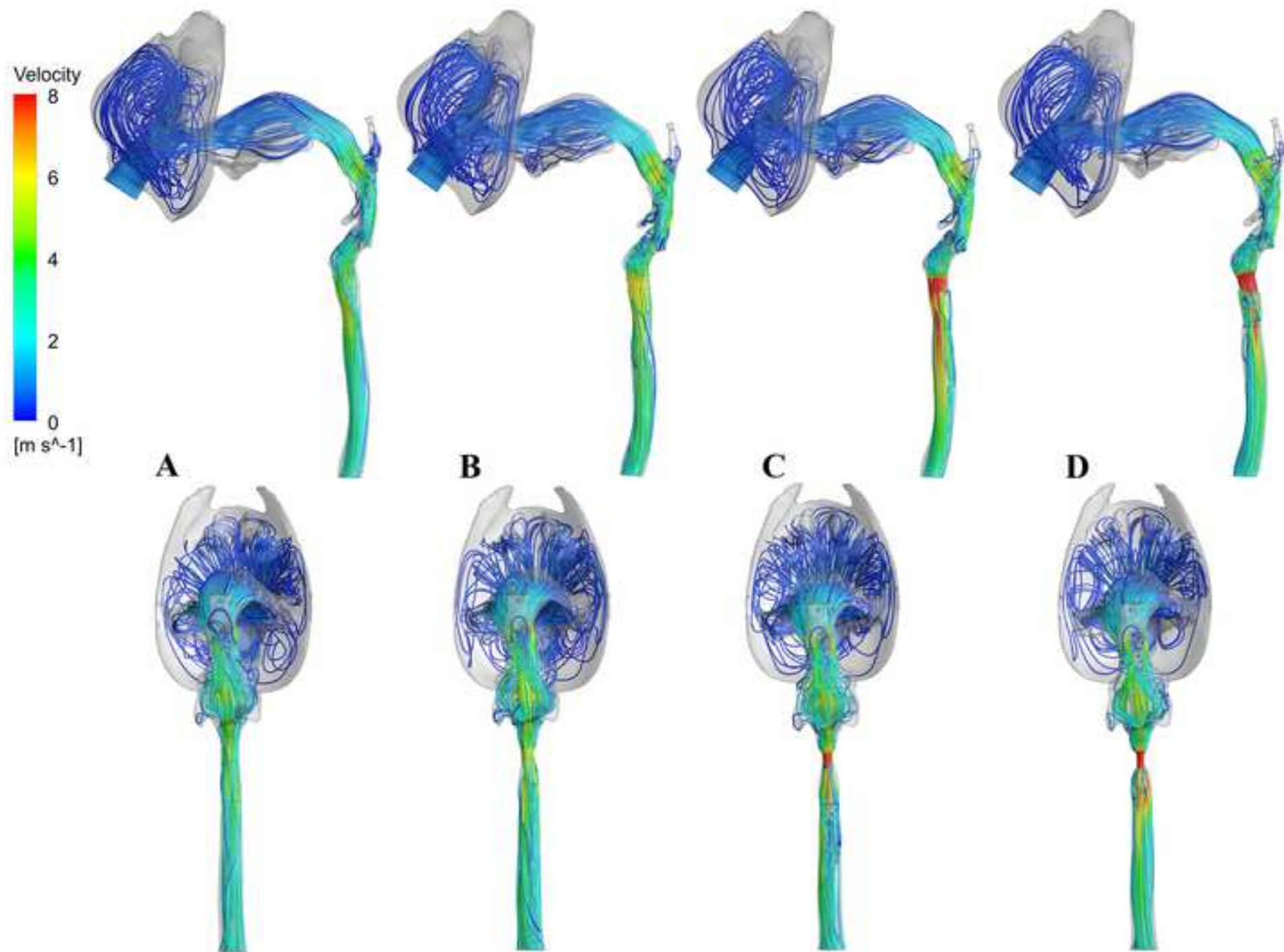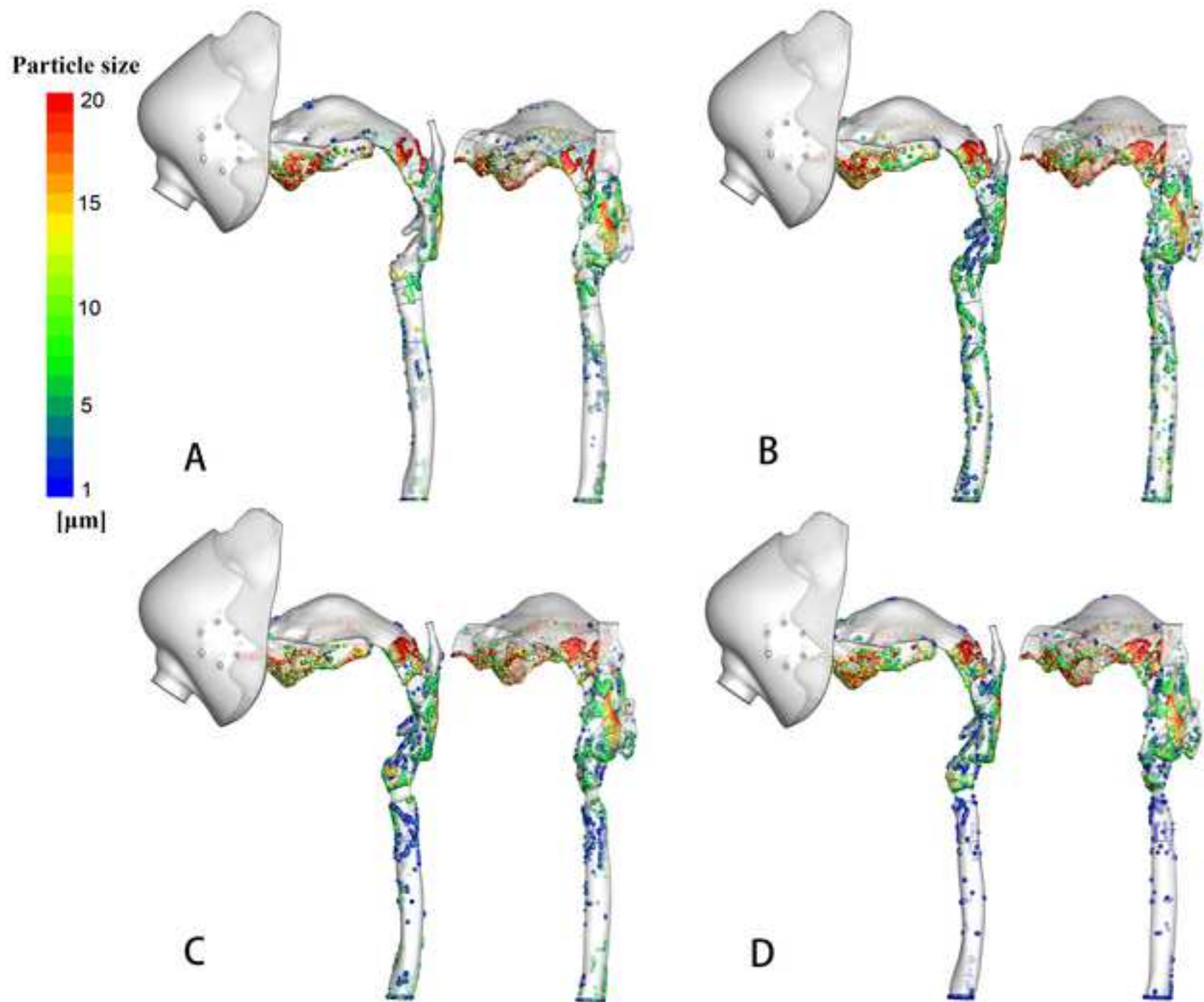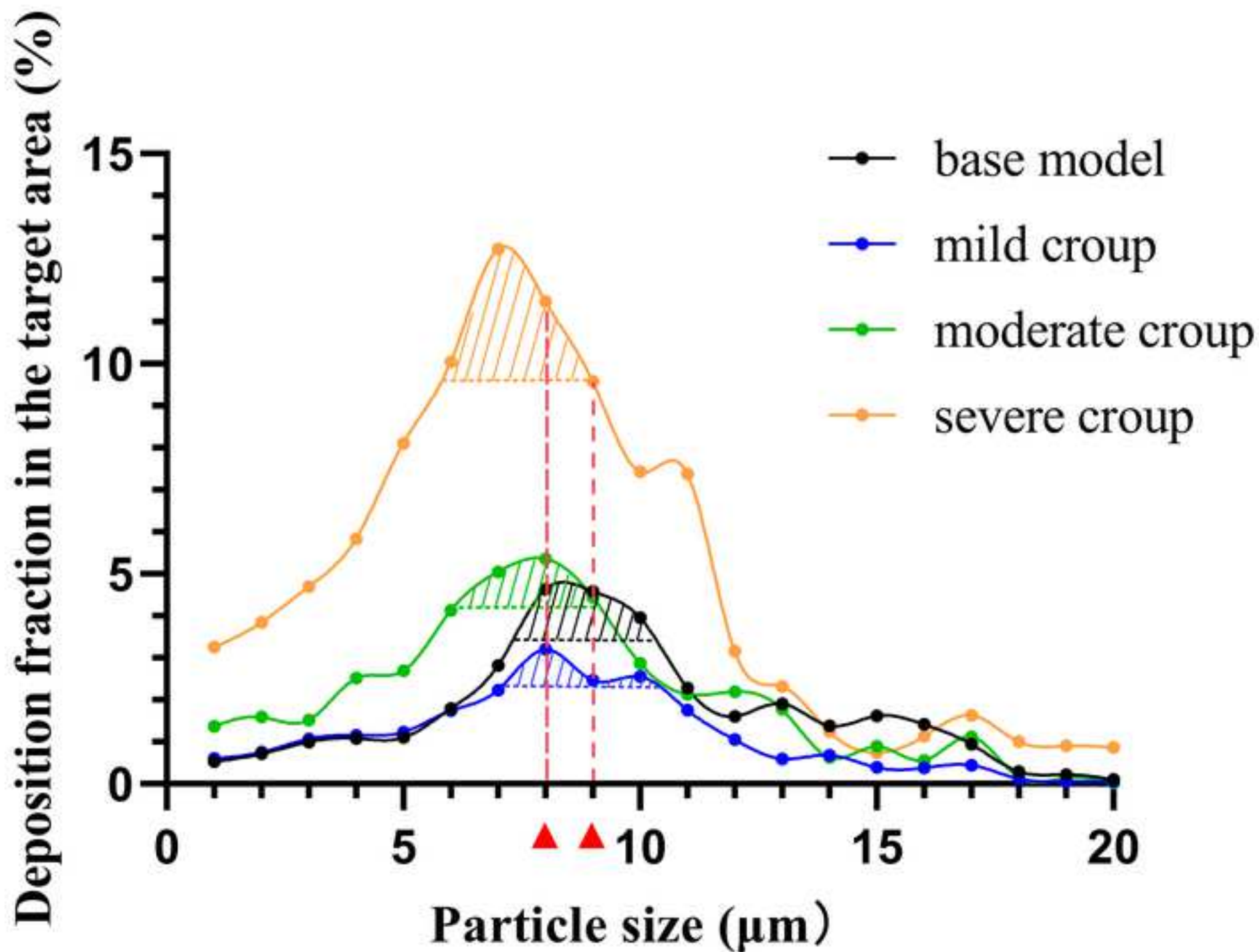
Figure 5

Figure 6

A   B   C   D
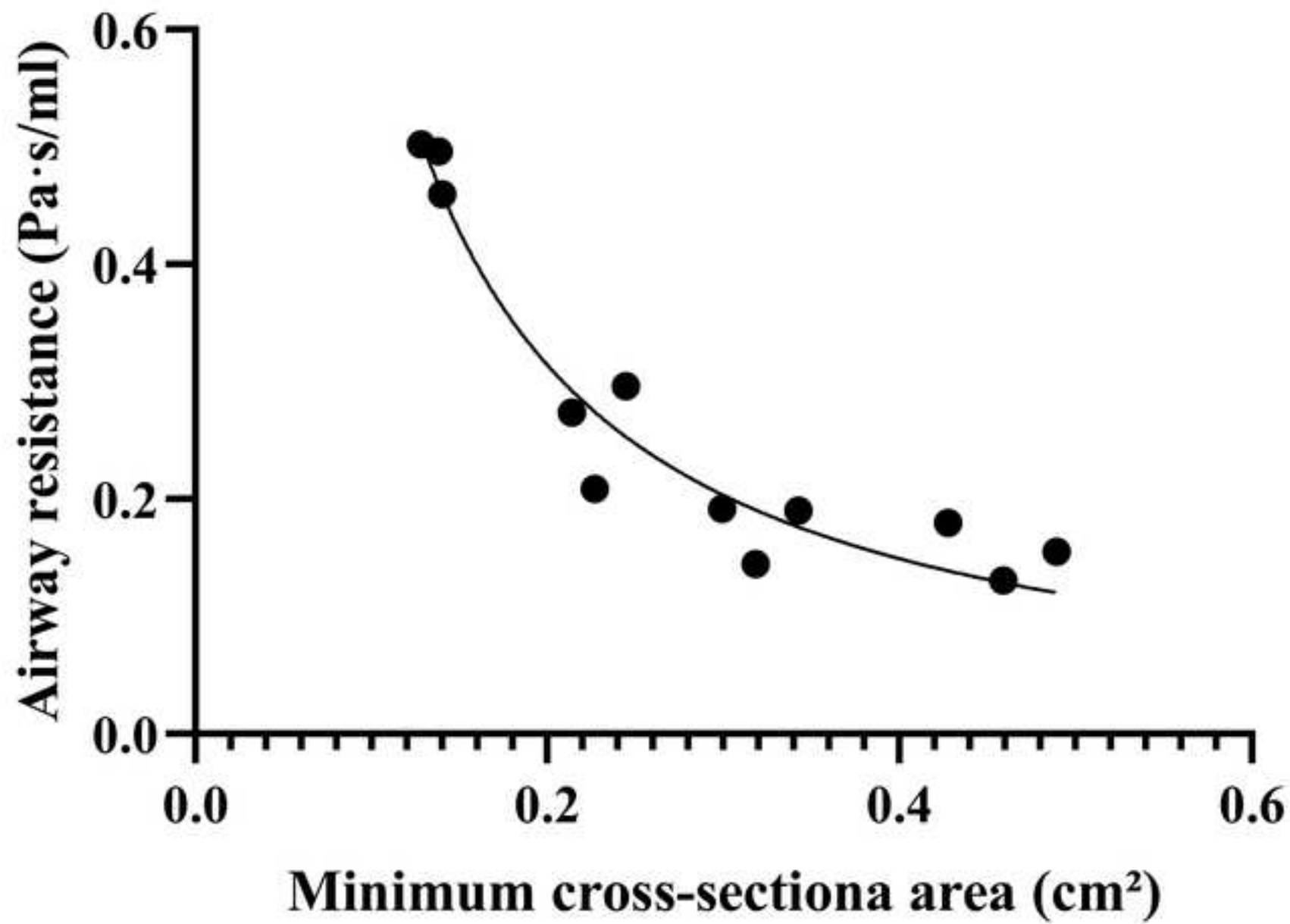
Figure 7

Figure 8

Figure 9

Figure 9

Figure 10

Click here to access/download;Figure;Figure 10.tif ⬇

Velocity
5.9

4.4

2.9

1.5

0.0
[m s^-1]

A 2μm   B 5μm   C 8μm   D 10μm   E 15μm   F 20μm